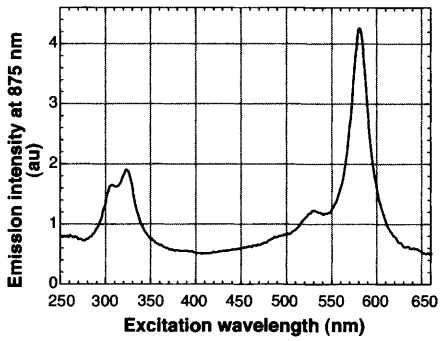

Fig. 4. Fluorescence excitation spectrum of the 875-nm band gap emission feature in a 296 K sample of fullerene nanotubes in 1% SDS in H_2O. The strong excitation feature at 581 nm is assigned as the second van Hove absorption of this nanotube species, appearing at an energy 1.51 times that of the first van Hove transition.

from protonated tubes in SDS micelles. This effect appears similar to the previously reported UV photodesorption of O_2 and other small molecules from single-walled nanotubes (*30*). PVP-wrapped nanotubes, dissolved either in water or in a solid film of PVP, show band gap luminescence efficiencies comparable to those of SDS-suspended samples.

The characteristic luminescence lifetime is found to be less than 2 ns, and we estimate a quantum yield on the order of 10^{-3}. Therefore, we classify the luminescence as fluorescence: spin-allowed emission from singlet excitons. This assignment is consistent with the very small spectral shift between absorption and emission, which also implies only minor geometrical differences between the ground and excited electronic states.

Optical excitation of a semiconducting nanotube in its second van Hove transition, E_{22}, will be followed by rapid electronic relaxation before emission in the first-branch transition, E_{11}. Therefore, by monitoring the intensity of a specific (first-branch) emission peak as a function of excitation wavelength within the second van Hove branch, one can identify the second-branch transition energy of the nanotube that gives that first-branch emission. Figure 4, which illustrates such an excitation spectrum for the 875-nm first-branch emission peak, shows a distinct, nearly lorentzian second-branch feature centered at 581 nm, giving a E_{22}/E_{11} value for this particular tube of 1.51. Extensive fluorescence excitation measurements, similar to Fig. 4, are now in progress for the entire range of emission features from these micelle-suspended tube samples. Early results show that the E_{22}/E_{11} ratio varies widely but averages to a value near 1.7, in contrast to the value of 2.0 predicted by tight binding theory (*2*). This difference may reflect nanotube exciton effects (*31*).

The observed nanotube fluorescence intensity was found to depend nonlinearly on the excitation intensity. Using 8-ns laser pulses at 532 nm, we observe that emission increases nearly linearly for energy densities below 0.1 mJ cm^{-2} but sublinearly at higher excitation levels, with an emission efficiency at 6 mJ cm^{-2} only ~25% of that found for weak excitation. Further studies will be needed to explore this nonlinear behavior, which probably reflects annihilating interactions between multiple excitons on individual nanotubes.

References and Notes

1. M. S. Dresselhaus, G. Dresselhaus, P. C. Eklund, *Science of Fullerenes and Carbon Nanotubes* (Academic Press, San Diego, 1996).
2. M. S. Dresselhaus, G. Dresselhaus, P. Avouris, Eds., *Carbon Nanotubes: Synthesis, Structure, Properties, and Applications*, vol. 80 (Springer, Berlin, 2001).
3. A. Thess *et al.*, *Science* **273**, 483 (1996).
4. L. A. Girifalco, M. Hodak, R. S. Lee, *Phys. Rev. B* **62**, 13104 (2000).
5. J. Liu *et al.*, *Science* **280**, 1253 (1998).
6. M. J. O'Connell *et al.*, *Chem. Phys. Lett.* **342**, 265 (2001).
7. S. Bandow *et al.*, *J. Phys. Chem. B* **101**, 8839 (1997).
8. J. Chen *et al.*, *Science* **282**, 95 (1998).
9. G. S. Duesberg, J. Muster, V. Krstic, M. Burghard, S. Roth, *Appl. Phys. A* **67**, 117 (1998).
10. A. B. Dalton *et al.*, *J. Phys. Chem. B* **104**, 10012 (2000).
11. A. B. Dalton *et al.*, *Synth. Metals* **121**, 1217 (2001).
12. R. Bandyopadhyaya, E. Nativ-Roth, O. Regev, R. Yerushalmi-Rozen, *Nano Lett.* **2**, 25 (2002).
13. M. J. Bronikowski, P. A. Willis, D. T. Colbert, K. A. Smith, R. E. Smalley, *J. Vacuum Sci. Technol. A* **19**, 1800 (2001).
14. R. Saito, G. Dresselhaus, M. S. Dresselhaus, *Physical Properties of Carbon Nanotubes* (Imperial College Press, London, 1998).
15. W. Zhou *et al.*, *Chem. Phys. Lett.* **350**, 6 (2001).
16. B. R. Brooks *et al.*, *J. Comput. Chem.* **4**, 187 (1983).
17. S. E. Feller, Y. Zhang, R. W. Pastor, *J. Chem. Phys.* **103**, 4613 (1995).
18. W. L. Jorgensen, *J. Am. Chem. Soc.* **103**, 335 (1981).
19. S. Bandyopadhyay, M. L. Klein, G. Martyna, J., M. Tarek, *Mol. Phys.* **95**, 377 (1998).
20. R. Saito, G. Dresselhaus, M. S. Dresselhaus, *Phys. Rev. B* **61**, 2981 (2000).
21. S. Reich, C. Thomsen, P. Ordejon, *Phys. Rev. B* **65**, 155411 (2002).
22. J. E. Riggs, Z. X. Guo, D. L. Carroll, Y. P. Sun, *J. Am. Chem. Soc.* **122**, 5879 (2000).
23. Y. Sun, S. R. Wilson, D. I. Schuster, *J. Am. Chem. Soc.* **123**, 5348 (2001).
24. E. C. Dickey *et al.*, *Appl. Phys. Lett.* **79**, 4022 (2001).
25. M. E. Brennan *et al.*, *Synth. Metals* **119**, 641 (2001).
26. Y. P. Sun *et al.*, *Chem. Phys. Lett.* **351**, 349 (2002).
27. Such a matched pattern implies a set of chromophores, each lacking vibrational structure in absorption and emission. Vibrational overtone emission would be undetectably weak under our conditions, and organic impurities would not emit in the near infrared.
28. T. W. Odom, J. L. Huang, P. Kim, C. M. Lieber, *Nature* **391**, 62 (1998).
29. J. W. G. Wildoer, L. C. Venema, A. G. Rinzler, R. E. Smalley, C. Dekker, *Nature* **391**, 59 (1998).
30. R. J. Chen *et al.*, *Appl. Phys. Lett.* **79**, 2258 (2001).
31. T. Ando, *J. Phys. Soc. Jpn.* **66**, 1066 (1997).
32. P. J. Karaulis, *J. Appl. Crystallogr.* **24**, 946 (1991).
33. D. J. Bacon, W. F. Anderson, *J. Mol. Graph.* **6**, 219 (1988).

34. Supported by the NSF Focused Research Group on Fullerene Nanotube Chemistry (DMR-0073046), the NSF Center for Biological and Environmental Nanotechnology (EEC-0118007), and the Robert A. Welch Foundation (C-0689). Support from NASA (NCC 9-77) for development of the HiPco method is also gratefully acknowledged. R.B.W. and S.M.B. are grateful to the NSF (grant CHE-9900417) and the Robert A. Welch Foundation (grant C-0807) for research support. We thank R. Saito for communicating unpublished computational results.

8 April 2002; accepted 4 June 2002

Increase in the Asian Southwest Monsoon During the Past Four Centuries

David M. Anderson,[1]* Jonathan T. Overpeck,[2] Anil K. Gupta[3]

Climate reconstructions reveal unprecedented warming in the past century; however, little is known about trends in aspects such as the monsoon. We reconstructed the monsoon winds for the past 1000 years using fossil *Globigerina bulloides* abundance in box cores from the Arabian Sea and found that monsoon wind strength increased during the past four centuries as the Northern Hemisphere warmed. We infer that the observed link between Eurasian snow cover and the southwest monsoon persists on a centennial scale. Alternatively, the forcing implicated in the warming trend (volcanic aerosols, solar output, and greenhouse gases) may directly affect the monsoon. Either interpretation is consistent with the hypothesis that the southwest monsoon strength will increase during the coming century as greenhouse gas concentrations continue to rise and northern latitudes continue to warm.

Major departures from normal seasonal rainfall seriously affect the agricultural output and economy of southwest Asia, which receives most of its annual rainfall during the summer monsoon season. Although decadal variations can be resolved in the instrumental record, little is known about centuries-long trends. Changes in the monsoon over thousands to millions of years can be reconstructed using sediments from the northwestern Arabian Sea, where upwelling driven by the monsoon winds deposits a unique fossil record. Changes in the monsoon over millions of years have been attributed to uplift of the Tibetan Plateau, which altered the

effective thermal contrast between land and sea (*1, 2*). Over tens of thousands of years, sediments from the Arabian Sea exhibit cycles of 23,000, 41,000, and 100,000 years, corresponding to insolation cycles driven by variations in the precession, obliquity, and eccentricity of Earth's orbit, respectively (*3–8*). Holocene reconstructions of the southwest Asian monsoon reveal a decrease in monsoon strength since a maximum 9000 to 6000 years ago (*9, 10*), consistent with forcing by the seasonal contrast in solar radiation [Northern Hemisphere summer radiation was 8% greater 9000 years ago than today (*11*)]. In addition to the direct effect of solar radiation, glacial boundary conditions (including expanded ice sheets and sea ice, cooler sea surface temperatures, and reduced atmospheric carbon dioxide) associated with the orbital cycles have been implicated in monsoon cyclicity (*6, 7, 12*). Investigations of millennial-scale Dansgaard-Oeschger (D-O) variability of the southwest monsoon have revealed a correspondence between cool intervals in the North Atlantic and diminished southwest monsoon strength as measured with proxies of Arabian Sea wind (*13, 14*). The link between cooler, or glacial, Northern Hemisphere climate and the southwest monsoon is not surprising, because both process-based studies (*15*) and observations (*16*) have shown that cooling and expanded snow cover over Eurasia reduces monsoon strength. On the basis of the observed link between cooling over Eurasia and the monsoon, we hypothesized that the cooling during the Little Ice Age may have weakened the southwest monsoon several hundred years ago. Similarly, an increase in East Asian monsoon precipitation in the past 500 years was tentatively attributed to Little Ice Age cooling (*17*).

Sediments from the Oman Margin are nannofossil-rich foraminifer oozes, produced each summer when strong southwest monsoon winds drive enhanced biological productivity in the northwestern Arabian Sea. Throughout most of the deep sea, bioturbation severely attenuates centennial-scale variability (*18, 19*), but in the Arabian Sea, low-oxygen conditions caused by high productivity prevent burrowing organisms from smoothing centennial-scale events. Although the sediments are not laminated, the potential to produce a long baseline of centennial-scale change still exists. The abundance (as a percentage of 41 species) of the foraminifer *G. bulloides* increases relative to other species with increased upwelling, as observed both geographically in core-top sediments (*20*) and in sediment-trap time series from the northwestern Arabian Sea (*21*). In the tropics, *G. bulloides* is present only in regions where upwelling occurs, and in these cases its abundance can exceed 60%. The large range and specific association with upwelling make *G. bulloides* an excellent proxy for upwelling driven by surface winds. This robust relation has been used as a proxy for wind velocity at several different times in the past in the Arabian Sea and in the Cariaco Basin (*22*).

We sampled two Soutar box subcores at continuous 2-mm spacing using the method developed for Cariaco Basin sediments (*22*) (supporting online text). Nine AMS (accelerator mass spectrometry) ^{14}C dates on planktonic foraminifers from core RC2730 provided the age control (fig. S1). When corrected for the average reservoir age of the Arabian Sea (*23, 24*), the uppermost four samples, including the replicated 0- to 2-mm sample, were too young (less than zero age), which can be explained by the presence of bomb radiocarbon that has mixed downward over the upper 10 mm (table S1). Each of the box core sediment surfaces was observed to be pristine during core recovery. This observation, combined with the presence of bomb radiocarbon in the upper samples, supports our assumption that the top of the box core corresponds to the date of collection (1986). We constructed an age model by fitting a line through 1986 at the core top and through the remaining reservoir-corrected, nonzero ^{14}C dates [the corrected age at zero depth (black symbol) in fig. S1 is the inferred age of –36 years (with respect to 1950)]. The date for 40 mm is too old to fit the linear sedimentation rate model, and we discounted this date because it comes from the minimum in *G. bulloides* abundance, where mixing could most easily bias the age. All the ^{14}C dates were determined on the core with the highest sedimentation rate (RC2730), and the second core was stratigraphically correlated to the dated core by a combination of the *G. bulloides*, calcium carbonate, and coarse fraction stratigraphies. We correlated 40 mm and 93 mm in RC2730 with 60 mm and 100 mm in RC2735 (Fig. 1). All upwelling indicators (percent carbonate, coarse fraction, and *G. bulloides*) reveal an increase in the most recent sediment. Dissolution is an unlikely explanation at least for the *G. bulloides* increase because *G. bulloides* is more resistant than the tropical foraminifers that constitute the assemblage. If the uppermost sediments were still dissolving, we would expect the *G. bulloides* concentration to be lower, not higher as observed. Uncertainty exists in the fine-scale stratigraphic correlation; however, longer carbonate stratigraphies indicate that sedimentation rates are roughly the same at each site over their 40-cm length (fig. S2) (*25*). Although the ^{14}C measurement uncertainty is less than 50 years, the uncertainty in the reservoir age of the Arabian Sea, combined with our assumption of linear sedimentation rate between dated intervals, probably yields an uncertainty on the order of ±100 years. The small amount of mixing indicated by the bomb radiocarbon may have smoothed the signal, incompletely mixing sediment over several millimeters (several decades). The frequency resolution and time uncertainty of this time series are similar to those of a typical terrestrial borehole temperature record (*26*).

The *G. bulloides* time series spans the last 1000 years (Fig. 2), and both cores show that

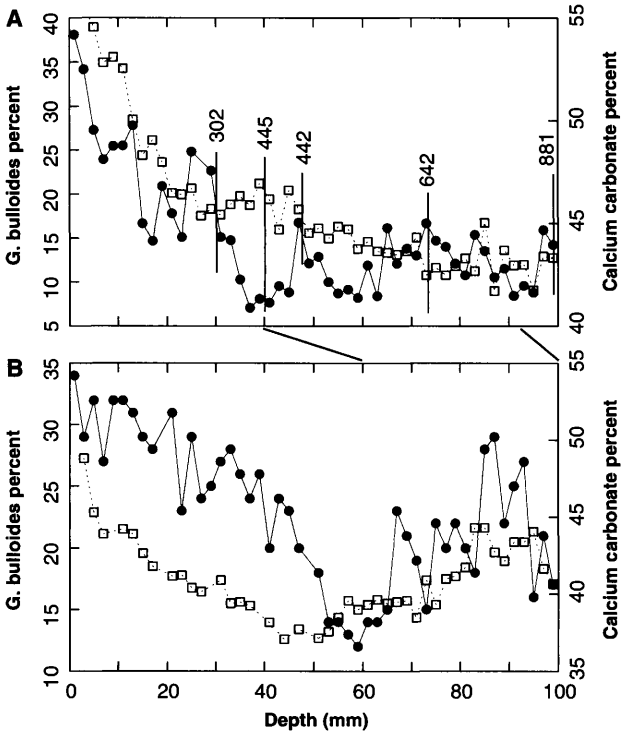

Fig. 1. Calcium carbonate (squares) and *G. bulloides* (circles) stratigraphy for RC2730 (**A**) and RC2735 (**B**). Also shown in (A) are the corrected AMS ^{14}C ages for RC2730. The correlation between RC2730 and RC2735 (shown by two lines between the panels) was made by correlating a combination of carbonate, *G. bulloides*, and coarse fraction events seen in both cores, also constrained by the 0- to 40-cm carbonate stratigraphy (fig. S2).

[1]NOAA Paleoclimatology Program and University of Colorado, Boulder, CO 80303, USA. [2]Department of Geosciences and Institute for the Study of Planet Earth, University of Arizona, Tucson, AZ 85721, USA. [3]Indian Institute of Technology, Kharagpur 721 302, India.

*To whom correspondence should be addressed. E-mail: dma@ngdc.noaa.gov

monsoon upwelling increased during the past four centuries. Longer records show that the lowest values (10%) observed in the Holocene occurred around 1600 (*3, 5*). The rate of the recent increase is not steady; a brief decrease in slope occurs between 1800 and 1900. In addition to the recent increase, there is a broader, centuries-long maximum that occurred between 1000 and 1500, with peak values from 1200 to 1400. We have low confidence in finer-scale events because of the dating uncertainty and the uncertainty in counting *G. bulloides* [the mean difference for duplicate counts is 3% (open circles with center point, Fig. 2A)]. To better constrain the magnitude of low-frequency change and reduce variation attributed to environmental variability in upwelling regions and to noise, we produced a composite record by averaging the values in both cores for 50-year intervals (thick line). The composite is our best estimate of the century-scale trend in *G. bulloides* during the past millennium (Fig. 2A) (table S2).

Interpreting the *G. bulloides* record in terms of wind speed change is complicated by the nonlinear relation between upwelling and wind speed. *G. bulloides* abundance does appear to be linearly related to upwelling, as demonstrated by the linear correlation between *G. bulloides* from core-top samples and sea surface temperature in the Arabian Sea (*27*), but the relation between upwelling (idealized here as the horizontal Ekman velocity away from the coast) is proportional to the square of the wind speed. Therefore, small changes in the wind speed result in much larger changes in the wind stress applied to the sea surface and hence larger changes in the *G. bulloides* population. This relation makes upwelling proxies an especially sensitive indicator of the surface wind and enhances the signal-to-noise ratio relative to other proxies. To interpret *G. bulloides* abundance as an indicator of the monsoon wind speed, we calculated the square root of the *G. bulloides* abundance difference from the 1975 average (34%) to produce the index likely to be linearly related to the monsoon wind speed (and thus the land-sea pressure gradient) (Fig. 2B) (table S2).

We compared the monsoon record with the reconstructed Northern Hemisphere temperature change (*28*) (Fig. 2B) and found that the broad features of the monsoon index are similar to the temperature reconstruction, namely, a slight decreasing trend from 1000 to 1500 followed by an increase in recent centuries. Other events that may be similar are the pause in the recent rate of increase between 1800 and 1900 and the acceleration of the rate of increase in the past century. Comparing the *G. bulloides* record directly to instrumental climate records is difficult because of the short length and large variance of the instrumental ship data. The trend since 1890 in the average Arabian Sea southwest monsoon wind speed (*29*) (16° to 22°N, 56° to 62°E, June-July-August average) is negligible, although the variance has decreased by 30% (perhaps as anemometer use increased). The trend in all-India rainfall, although positive, is small and statistically insignificant (*30, 31*); however, the regional (*32*) and year-to-year variability is large (10%). Using historical data, Mooley and Pant (*33*) found no change in the last 200 years in the frequency of extreme drought events; however, it is not certain that extreme drought events should correlate directly with the upwelling index. We found no instrumental evidence suitable to verify or reject the increasing trend observed in 50-year averages for 1875, 1925, and 1975.

There are several mechanisms that might link the monsoon with Northern Hemisphere temperature change over the past 1000 years. Instrumental observation (*16, 34*) and modeling studies (*10, 15*) have shown that cooling or increased snow cover in Asia acts to weaken the monsoon in the following year. Overpeck *et al.* (*10*) showed that cooler North Atlantic sea surface temperatures can contribute to the cooling downstream over Asia and monsoon weakening. Geologic studies over a range of time scales support the hypothesis that glacial (and D-O cycle) cooling weakens the monsoon (*13, 14, 35*). Similar changes may have occurred over the past 1000 years—for example, during the Little Ice Age, when Europe was cooler than at present. Alternatively, the forcing hypothesized to affect Northern Hemisphere temperature (volcanic aerosols, solar output, greenhouse gas change) may have directly altered the land-sea pressure contrast that drives the Asian monsoon. The mid-1600 to mid-1700 period corresponds to the time of the Maunder minimum in solar activity (*24*), consistent with direct solar forcing of the monsoon. Unfortunately, the *G. bulloides* record is not sufficiently resolved to discriminate among these forcing time series. In the past few decades, the premonsoon surface temperatures over Eurasia have exceeded the warming in the Indian Ocean, thus increasing the land-sea thermal contrast conducive for a strong southwest monsoon. The instrumental observations strengthen our conclusion that over the past four centuries, a warming trend over Eurasia has enhanced the southwest monsoon. The evidence supports either a link between the monsoon and northern warming, or a direct effect of temperature forcing (by volcanic aerosols, solar output, or greenhouse gas change) on the monsoon. One possibility is that volcanic, solar, or greenhouse gas changes that affect northern warming lead, in turn, to changes in the southwest monsoon via the monsoon–snow cover link.

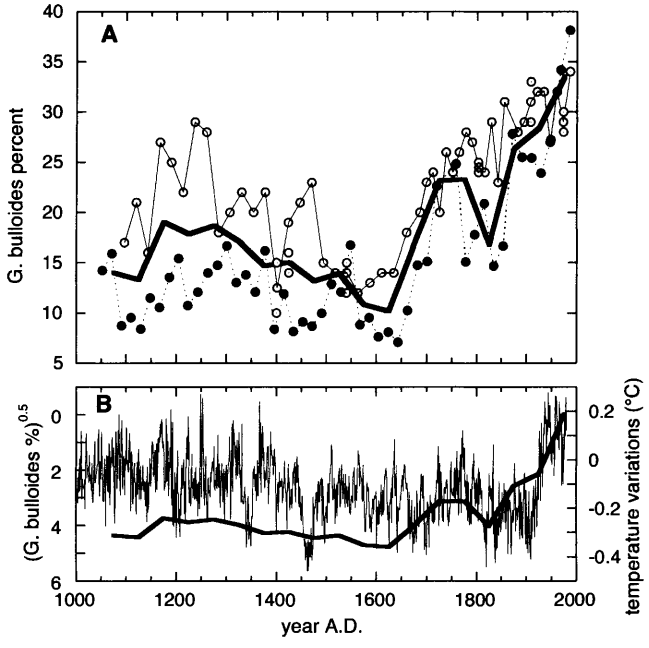

Fig. 2. (**A**) Time series of *G. bulloides* abundance from box cores RC2730 (solid circles) and RC2735 (open circles), and the composite record produced by averaging samples within 50-year intervals during the past 1000 years (thick line). Duplicate counts are indicated by open circles with a center point. (**B**) Time series of Northern Hemisphere temperature variations from (*28*) (thin line) superimposed on the index linearly related to monsoon wind speed, the square root of the difference in composite *G. bulloides* abundance with respect to the 1975 average (thick line).

The monsoon record of the past 1000 years encompasses an important period of medieval, modern, and independent Indian history, which is marked by crucial political and socioeconomic changes in the region. The upwelling data are relevant because they reveal that the century-scale changes and long-term trend are large compared to the statistically insignificant trend observed in the 140-year instrumental record. The monsoonal changes have important implications for the human population of South Asia; for instance, a pause in the southwest monsoon at about 1800 to 1900 (Fig. 2A) closely corresponds to a major famine in India in 1877 (*36*). Historical climatic records from South Asia are rare; however, the coldest period of the past 400 years in western China was ~1600 to 1670 (*37, 38*), coinciding with the weakest southwest monsoon. The impact of this cold and dry phase is also observed in the northern Indian Himalayan states (Kashmir and Sikkim) and eastern Asia (*37, 39*). Before this time (950 to 1290), evidence from Maili Bog in northwestern China

is interpreted to indicate a stronger monsoon (*40*). Morrill *et al.* summarized evidence for an abrupt monsoon shift around 1300 that is heterogeneous in geographical extent (*41*). The centuries-long increase in the southwest monsoon between 1000 and 1500 coincides with a wet phase in India, as observed in the speleothem data from central and eastern regions of the country (*42*). Although these studies support the major trends in our record, more data are needed to test our hypothesized changes in monsoon strength over the past 1000 years, particularly over Tibet and regions of India strongly affected by the southwest monsoon.

References

1. W. L. Prell, D. Murray, S. C. Clemens, D. M. Anderson, in *Synthesis of Results from Scientific Drilling in the Indian Ocean*, R. A. Duncan *et al.*, Eds. (Geophysical Monograph 70, American Geophysical Union, Washington, DC, 1992), pp. 447–469.
2. Z. T. Guo *et al.*, *Nature* **416**, 159 (2002).
3. M. A. Altabet, R. Francoise, D. M. Murray, W. L. Prell, *Nature* **373**, 506 (1995).
4. J. E. Kutzbach, F. A. Street-Perrott, *Nature* **317**, 130 (1985).
5. S. C. Clemens, W. L. Prell, D. W. Murray, G. Shimmield, G. Weedon, *Science* **353**, 720 (1991).
6. S. C. Clemens, D. W. Murray, W. L. Prell, *Science* **274**, 943 (1996).
7. D. M. Anderson, W. L. Prell, *Paleoceanography* **8**, 193 (1993).
8. G. J. Reichart, L. J. Lourens, W. J. Zachariasse, *Paleoceanography* **13**, 607 (1998).
9. P. D. Naidu, B. J. Malmgren, *Paleoceanography* **11**, 129 (1996).
10. J. T. Overpeck, D. M. Anderson, S. Trumbore, W. L. Prell, *Clim. Dyn.* **12**, 213 (1996).
11. COHMAP Project Members, *Science* **241**, 1043 (1988).
12. F. Sirocko *et al.*, *Nature* **364**, 322 (1993).
13. M. A. Altabet, M. J. Higginson, D. W. Murray, *Nature* **415**, 159 (2002).
14. F. Sirocko, D. Garbe-Schonberg, A. McIntyre, B. Molfino, *Science* **272**, 526 (1996).
15. G. A. Meehl, *Science* **266**, 263 (1994).
16. T. P. Barnett, L. Dumenil, U. Schlese, E. Roeckner, M. Latif, *J. Atmos. Sci.* **46**, 661 (1989).
17. L. Wang *et al.*, *Geophys. Res. Lett.* **26**, 2889 (1999).
18. D. M. Anderson, *Paleoceanography* **16**, 352 (2001).
19. T. J. Goreau, *Nature* **287**, 620 (1980).
20. W. L. Prell, in *Climate Processes and Climate Sensitivity*, J. E. Hansen, T. Takahashi, Eds. (American Geophysical Union, Washington, DC, 1984), pp. 48–57.
21. W. B. Curry, D. R. Ostermann, M. V. S. Guptha, V. Ittekkot, in *Upwelling Systems: Evolution Since the Early Miocene*, C. P. Summerhayes, W. L. Prell, K. C. Emeis, Eds. (Geological Society, London, 1992), pp. 93–106.
22. D. E. Black *et al.*, *Science* **286**, 1709 (1999).
23. M. Stuiver, P. J. Reimer, *Radiocarbon* **35**, 15 (1993).
24. M. Stuiver, T. F. Braziunas, *Radiocarbon* **35**, 137 (1993).
25. D. M. Anderson, thesis, Brown University (1991).
26. S. Huang, H. N. Pollack, P.-Y. Shen, *Nature* **403**, 756 (2000).
27. W. L. Prell, in *Milankovitch and Climate, Part 1*, A. L. Berger *et al.*, Eds. (American Geophysical Union, Washington, DC, 1984), pp. 48–57.
28. M. E. Mann, R. S. Bradley, M. K. Hughes, *Geophys. Res. Lett.* **26**, 759 (1999).
29. R. J. Slutz *et al.*, *Comprehensive Ocean-Atmosphere Data Set; Release 1* (Climate Research Program, Boulder, CO, 1985).
30. B. Parthasarathy, A. A. Munot, D. R. Kothawale, *Theor. Appl. Climatol.* **49**, 217 (1994).
31. K. Y. Vinnikov, A. Robock, *Geophys. Res. Lett.* **29**, 1029 (2002).
32. I. Subbaramayya, C. V. Naidu, *Int. J. Climatol.* **12**, 597 (1992).
33. D. A. Mooley, G. B. Pant, in *Climate and History*, T. M. L. Wigley, M. S. Ingram, G. Farmer, Eds. (Cambridge Univ. Press, Cambridge, 1981), pp. 465–478.
34. M. Sankar-Rao, K. M. Lau, S. Yang, *Int. J. Climatol.* **16**, 605 (1996).
35. S. C. Porter, A. Zhisheng, *Nature* **375**, 305 (1995).
36. W. J. Burroughs, *Does the Weather Really Matter? The Social Implications of Climatic Change* (Cambridge Univ. Press, Cambridge, 1997).
37. P. D. Jones, R. S. Bradley, in *Climate Since A.D. 1500*, R. S. Bradley, P. D. Jones, Eds. (Routledge, New York, 1992), pp. 649–665.
38. G. C. Jacoby, R. D. D'Arrigo, T. Davaajamts, *Science* **273**, 771 (1996).
39. C. Sharma, M. S. Chauhan, *J. Paleontol. Soc. India* **46**, 51 (2001).
40. G. Ren, *Geophys. Res. Lett.* **25**, 1931 (1998).
41. C. Morrill, J. T. Overpeck, J. E. Cole, in preparation.
42. M. G. Yadava, R. Ramesh, *J. Sci. Industr. Res.* **58**, 339 (1999).

Supporting Online Material

www.sciencemag.org/cgi/content/full/297/5581/596/DC1
Supporting Text
Figs. S1 and S2
Tables S1 and S2

15 April 2002; accepted 6 June 2002

Fork Reversal and ssDNA Accumulation at Stalled Replication Forks Owing to Checkpoint Defects

José M. Sogo,[1]* Massimo Lopes,[2]* Marco Foiani[2]†

Checkpoint-mediated control of replicating chromosomes is essential for preventing cancer. In yeast, Rad53 kinase protects stalled replication forks from pathological rearrangements. To characterize the mechanisms controlling fork integrity, we analyzed replication intermediates formed in response to replication blocks using electron microscopy. At the forks, wild-type cells accumulate short single-stranded regions, which likely causes checkpoint activation, whereas *rad53* mutants exhibit extensive single-stranded gaps and hemi-replicated intermediates, consistent with a lagging-strand synthesis defect. Further, *rad53* cells accumulate Holliday junctions through fork reversal. We speculate that, in checkpoint mutants, abnormal replication intermediates begin to form because of uncoordinated replication and are further processed by unscheduled recombination pathways, causing genome instability.

Chromosome integrity during DNA replication is essential for preventing genome rearrangements and cancer (*1–3*). When replication pauses, the stability of stalled forks is controlled by the checkpoint (*4*, *5*), which, in *Saccharomyces*, requires Rad53 kinase activation (*6*). Active Rad53 somehow prevents accumulation of abnormal intermediates allowing the forks to restart DNA synthesis (*4*, *7*, *8*). Hydroxyurea-treated *rad53* cells accumulate DNA structures that impede replication resumption when the inhibitor is removed (*4*).

In vivo psoralen cross-linking and electron microscopy (*9*) were used to analyze these intermediates. Samples from hydroxyurea-treated wild-type and *rad53* cells were cross-linked with psoralen (*10*), enriched in replication intermediates by binding and elution from BND cellulose (benzoylated naphthoylated DEAE cellulose), and analyzed by electron microscopy under nondenaturing and denaturing conditions.

Wild-type cells exhibit replicating bubbles with normal forks (Fig. 1A). Conversely, ~75% of the replication intermediates in *rad53* cells contained large single-stranded regions at the forks (Fig. 1, B to D). We frequently found bubbles with gaps in both leading or both lagging strands (Fig. 1B). In 40% of the replication intermediates, one parental strand is replicated, whereas the complementary parental strand remains single-stranded (hemi-replicated molecules; Fig. 1, C and F; table S1). We also found adjacent bubbles (Fig. 1D), likely due to firing of pseudo or dormant (*11*, *12*) origins of replication. Again, most of the bubbles were hemi-replicated (Fig. 1D). In wild-type cells bubble size increases with time (Table 1), whereas the single-stranded regions remain constant [~320 nucleotides (nt), Fig. 1E, table S1]. In *rad53* cells, bubbles exhibit a marginal increase in size (Table 1), whereas the extent of the single-stranded regions roughly doubles (Fig. 1E, table S1). In wild-type cells, the ratio between bubbles and

[1]Institute of Cell Biology, ETH Hönggerberg, CH-8093 Zürich, Switzerland. [2]Istituto F.I.R.C. di Oncologia Molecolare, Via Adamello 16, 20141, Milano, Italy, and Dipartimento di Genetica e di Biologia dei Microrganismi, Università degli Studi di Milano, Via Celoria 26, 20133, Milano, Italy.

*These authors contributed equally to this work.
†To whom correspondence should be addressed. E-mail: foiani@ifom-firc.it